

CrossMark
click for updatesCite this: *J. Mater. Chem. A*, 2015, 3, 20080Received 3rd August 2015
Accepted 10th September 2015

DOI: 10.1039/c5ta06018d

www.rsc.org/MaterialsA

Nanoflower-like metallic conductive MoO₂ as a high-performance non-precious metal electrocatalyst for the hydrogen evolution reaction†

Yanshuo Jin and Pei Kang Shen*

Searching for non-precious metal electrocatalysts with high activity and stability for the hydrogen evolution reaction (HER) has attracted considerable attention. Herein, we report the synthesis of nanoflower-like MoO₂ on nickel foam (NFL MoO₂/NF). Remarkably, as a HER electrocatalyst operating in alkaline electrolytes, NFL MoO₂/NF exhibits high stability and activity. The onset potential of NFL MoO₂/NF is almost 0 V *versus* the reversible hydrogen electrode (RHE) and bubbles can be produced on the surface of NFL MoO₂/NF under a static overpotential of only 10 mV, comparable to commercial Pt/C. NFL MoO₂/NF needs overpotentials of only about 55 and 80 mV to achieve current densities of 10 and 20 mA cm⁻², respectively. NFL MoO₂/NF has superior stability in the long-term electrochemical process and retains 94.3 percent of its initial current density after 25 hours.

Introduction

Hydrogen has been proposed as an alternative to diminishing fossil fuels.¹ Electrolysis of water into hydrogen and oxygen in an electrolyzer is the simplest way to produce high-purity hydrogen.² Nickel (Ni) is typically used in industry for water electrolysis in alkaline solution but with a high overpotential and large Tafel slope.³ Platinum (Pt) and its alloys are the best HER catalysts, but the cost and scarcity of Pt are serious impediments to their large-scale industrial application for electrolysis.^{4,5} These disadvantages have motivated many research efforts and some active and stable non-precious metal-based HER catalysts have been pursued in the past few years.^{6,7} Molybdenum based non-precious-metal compounds have been intensively studied for HER catalysts, including MoS₂,^{8–12} MoSe₂,^{8,13} MoB,¹⁴ Mo₂C,^{14–18} MoP^{19,20} and so on.

According to the literature data, molybdenum based metallic transition metal oxide MoO₂ crystallizes in a monoclinic cell and has a distorted rutile structure.²¹ The bonding is complex and involves delocalization of some of the Mo electrons in the conduction band accounting for the metallic conductivity.²¹ Tungsten based metallic transition metal oxide WO₂ has the same distorted rutile crystal structure as MoO₂ and exhibits excellent performance for H₂ generation: the onset overpotential is only 35 mV.²² Thus, metallic transition metal oxides are potential candidates for electrocatalysts for the hydrogen evolution reaction.

Polymer binders (Nafion or PTFE) are usually used to immobilize catalysts on the electrode surface for electrochemical measurements and practical applications.²³ However, the whole process is time-consuming and the polymer binder may reduce effective catalytic activity because it blocks active sites and reduces gas permeability and increases the mass transfer overpotential.²⁴ Thus, the problem can be solved by synthesizing electrocatalytic nanomaterials on substrates without binder.²⁵

Herein, we report on our recent efforts in developing a novel nanoflower-like MoO₂ on nickel foam (NF). The nanoflower-like MoO₂·2H₂O precursor was first directly grown on commercial nickel foam (NFL MoO₂·2H₂O/NF) by a wet-chemical route. An annealing treatment at 500 °C in a N₂ atmosphere and a subsequent annealing treatment at 400 °C in a H₂ atmosphere were used to synthesize NFL MoO₂/NF. As an integrated non-precious metal high-performance cathode for generating hydrogen from alkaline solutions, the NFL MoO₂/NF maintains its activity for at least 50 hours and shows an onset potential of almost 0 V and a Tafel slope of 66 mV dec⁻¹. NFL MoO₂/NF needs overpotentials of only about 55 and 80 mV to achieve current densities of 10 and 20 mA cm⁻², respectively. The large exchange current density (~1.8 mA cm⁻²) of NFL MoO₂/NF can be associated with its high surface area, corresponding to many more active sites exposed for the HER.

State Key Laboratory of Optoelectronic Materials and Technologies, School of Physics and Engineering, Sun Yat-sen University, Guangzhou, 510275, P. R. China. E-mail: stsspk@mail.sysu.edu.cn

† Electronic supplementary information (ESI) available. See DOI: 10.1039/c5ta06018d

Experimental

Materials

Ammonium molybdate tetrahydrate ((NH₄)₆Mo₇O₂₄·4H₂O), hydrochloric acid (HCl), potassium hydroxide (KOH) and Ni foam were purchased from Dongzheng Ltd. All chemical reagents used in this experiment were of analytical grade. The water used throughout all experiments was purified through a Millipore system.

Synthesis of NFL MoO₂·2H₂O/NF

Two Ni foams (40.0 mm × 20.0 mm × 1.0 mm) were cleaned with diluted hydrochloric acid, ethanol and deionized water several times. Then, 20 mmol L⁻¹ (NH₄)₆Mo₇O₂₄·4H₂O were dissolved in 35 mL deionized water at room temperature to form a uniform solution. The solution was subsequently transferred into a 50 mL Teflon-lined stainless steel autoclave, and the pre-treated Ni foams were placed upright in the autoclave. The autoclave was heated to 100 °C in an electric oven and maintained for 18 h, after that the Ni foams with the precursor were cleaned with deionized water several times before being fully dried in air at 60 °C.

Synthesis of NFL MoO₂/NF

NFL MoO₂·2H₂O/NF was annealed in N₂ at 500 °C for 1 h and subsequently in H₂ at 400 °C for 1 h.

Synthesis of NFL MoO₂(MoO₃)/NF

NFL MoO₂·2H₂O/NF was annealed in N₂ at 500 °C for 1 h.

Calculated MoO₂ loading

NFL MoO₂/NF was immersed in a 35% HCl solution for one day, and then was filtered, dried and weighed.

Characterization

Powder XRD data were acquired on a D-MAX 2200 VPC diffractometer with Cu K α radiation (λ = 1.54056 Å). The Raman spectrum was recorded on a micro-Raman system (Renishaw, in via). The IR spectrum was recorded on a Nicolet6700/Thermo/America Fourier transform infrared spectrometer. DSC of the products was carried out on a DSC-204/Netzsch/Bruke differential scanning calorimeter. SEM measurements were carried out on a Quanta 400/INCA/HKL scanning electron microscope at an accelerating voltage of 30 kV. TEM measurements were performed on a Tecnai G2 F30 transmission electron microscope at 300 kV. XPS measurements were performed on an ESCALAB 250 system.

Electrochemical measurements

The electrochemical measurements were conducted in a typical three-electrode setup with a reversible hydrogen electrode (RHE) as the reference electrode and a graphite rod as the counter electrode. Steady-state potential polarization curves were measured in 1 M KOH solution at different temperatures.

Accelerated degradation measurements were conducted for 3000 cyclic voltammetry (CV) cycles in 1 M KOH solution at a scan rate of 50 mV s⁻¹ and linear sweep voltammetry (LSV) measurements were conducted at a scan rate of 1 mV s⁻¹. Electrochemical impedance spectroscopy (EIS) experiments were performed with a three-electrode cell system in 1 M KOH at 25 °C. The potentiostat was operated over a frequency range of 1 kHz–100 mHz in a 10.0 mV AC voltage.

Results and discussion

After hydrothermal treatment, a nanoflower-like precursor is grown on the Ni foam which changes in color from silver-grey to reddish brown and then the color changes to black after annealing treatments (Fig. S1, ESI†). Fig. 1a shows the X-ray diffraction (XRD) pattern of the NFL MoO₂/NF, the peaks assigned to monoclinic MoO₂ (PDF#65-5787) were detected. The strong peaks at 44.5°, 51.8°, and 76.4° originate from the Ni foam substrate (PDF#65-2865). Fig. 1b shows the Raman spectrum and the monoclinic MoO₂ was detected with Raman bands at 200, 226, 345, 351, 456, 492, 569 and 739 cm⁻¹.²⁶

Fig. S2, ESI† shows the scanning electron microscopy (SEM) images of nanoflower-like precursor/Ni foam, indicating that the entire surface of the Ni foam is uniformly covered by the nanoflower-like/calyx-type precursor. The IR spectrum of the precursor is consistent with the standard spectrum of molybdenum dioxide. As shown in Fig. S3a, ESI† the intense band at 950 cm⁻¹ is assigned to $\nu(\text{Mo}=\text{O})$, while the prominent bands in the range of 500–850 cm⁻¹ are attributed to $\nu(\text{Mo}-\text{O}-\text{Mo})$. In addition, the broad band at 3210 cm⁻¹ and 1610 cm⁻¹ corresponds to the absorbed water.²⁷ Fig. S3b† shows the XRD pattern of the precursor, but it is still hard to judge what the precursor is. The TG and DTA curves of the precursor in a N₂ atmosphere are shown in Fig. S4, ESI† It shows two major events. The endothermic peak and exothermic peak at 121 °C and 485 °C on the DTA curve give two thermal behaviors. The broad endothermic peak on the DTA curve at about 121 °C corresponds to the release of the adsorbed water.²⁷ The sharp exothermic peak at 485 °C is associated with the formation of crystalline MoO₂ in the N₂ atmosphere (Fig. S5, ESI†), it is the same as the data reported in the literature.²⁷ The mass loss of 21% corresponds to the loss of almost two absorbed water molecules (theoretical value 22%) and we can deduce that the precursor is MoO₂·2H₂O. So we can conclude that the reaction

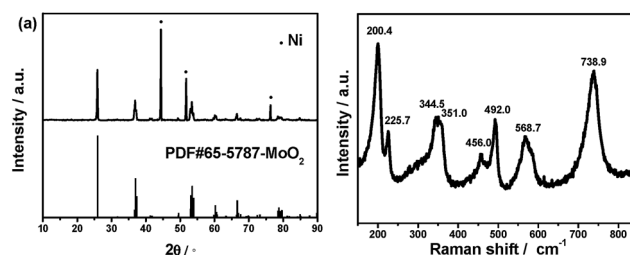
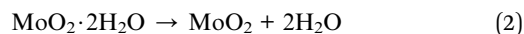
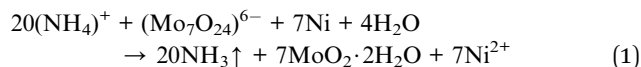


Fig. 1 (a) XRD pattern and (b) Raman spectrum of NFL MoO₂/NF.

mechanism is expressed by eqn (1) and eqn (2) in the hydrothermal synthesis reactor and the tube furnace, respectively.



Scanning electron microscopy (SEM, Fig. 2a and b) images of NFL MoO₂/NF show that the nanoflower-like morphology is preserved and the entire surface of the nickel foam is uniformly covered by nanoflower-like MoO₂. A close view of nanoflower-like MoO₂ (Fig. 2c) reveals that the nanoflower-like morphology consists of many nanosheets and the bulk MoO₂ plays a role in linking nanoflower-like MoO₂ and nickel foam. The nanoflower-like structure could lead to a much higher surface area than bulk materials, so the nanoflower-like structure contributed the majority of the active sites exposed for the HER. The corresponding energy dispersive X-ray (EDX) spectrum (Fig. S6, ESI†) verifies the 1 : 2 atomic ratio of Mo to O. The skeletal structure of the Ni foam was maintained completely, thus enabling its direct use as an integrated three-dimensional cathode for the HER. Transmission electron microscopy (TEM, Fig. 3a) and high-resolution (HR) TEM (Fig. 3b) images show that the nanoflower-like MoO₂ consists of many nanoparticles, forming lamellar superstructures at the micrometer scale. The HRTEM image shows well-resolved lattice fringes with an interplanar distance of 0.48 nm, which correspond to the (100) plane of the MoO₂. A high-angle annular dark-field scanning transmission electron microscopy (HAADF-STEM) image and the corresponding energy-dispersive X-ray (EDX) mapping (Fig. 3c) showed that the Mo and O atoms were distributed homogeneously.

Fig. 4a shows the steady-state potential polarization curves of Ni foam, commercial 46.7% Pt/C (TKK, Japan, loading: 0.2 mg cm⁻²) and NFL MoO₂/NF (MoO₂ loading: ~4.5 mg cm⁻²) in N₂-saturated 1 M KOH solution at 25 °C. In sharp contrast, NFL MoO₂/NF is significantly active for the HER with an onset overpotential of almost 0 V, and an additional negative potential leads to a rapid increase in the cathodic current. This value is superior to most of the reported values for non-precious-metal HER electrocatalysts (Table S1, ESI†). In addition, NFL MoO₂/NF needs overpotentials of only about 55 and 80 mV to achieve current densities of 10 and 20 mA cm⁻², respectively. The inset picture in Fig. 4a shows bubbles on NFL MoO₂/NF

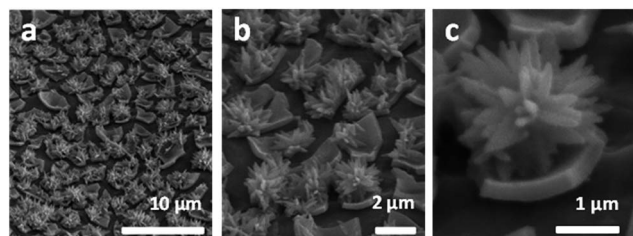


Fig. 2 (a–c) SEM images with different magnifications of the NFL MoO₂/NF.

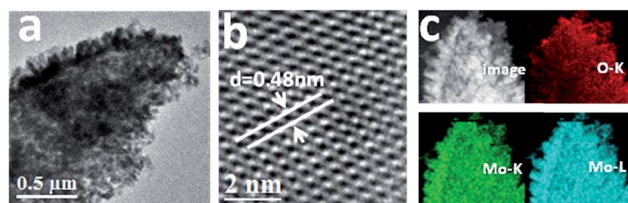


Fig. 3 (a) TEM image and (b) HRTEM image of MoO₂ and (c) STEM image and the corresponding EDX elemental mapping images of O and Mo for MoO₂.

after a steady-state overpotential of only 10 mV for several minutes and Movie S1† shows a HER movie on NFL MoO₂/NF under steady-state overpotentials of only 10 mV and 50 mV. Both of them show bubbles produced on the surface of NFL MoO₂/NF under steady-state overpotentials, indicating that the onset potential is smaller than 10 mV. The Tafel slopes were 29 mV dec⁻¹, 66 mV dec⁻¹ and 117 mV dec⁻¹ for commercial 46.7% Pt/C, NFL MoO₂/NF and Ni foam, respectively (Fig. 4b). The Tafel slope for NFL MoO₂/NF indicated that the HER proceeds by a Volmer–Heyrovsky mechanism.²⁸ By using the extrapolation method on the Tafel plots, the exchange current density (*j*₀) of NFL MoO₂/NF was calculated to be 1.8 mA cm⁻².

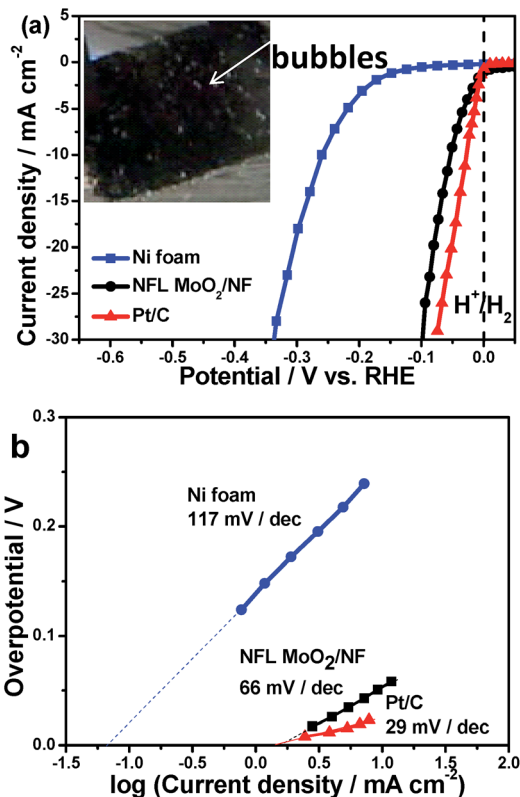


Fig. 4 (a) Steady-state polarization curves for Ni foam, NFL MoO₂/NF and commercial Pt/C in 1 M KOH. The inset picture in (a) shows hydrogen bubbles on NFL MoO₂/NF under a steady-state potential of only 10 mV for several minutes. (b) Tafel plots for Ni foam, NFL MoO₂/NF and commercial Pt/C in 1 M KOH.

Furthermore, electrochemical impedance spectroscopy (EIS) experiments were carried out to study the electrode kinetics of the HER. Fig. S7, ESI† shows the Nyquist plots of the impedance of different catalysts at different overpotentials. The absence of Warburg impedance indicates that the reaction is kinetically controlled; while the presence of only one semicircle in each Nyquist plot reveals that the equivalent circuit for the HER is characterized by one time constant.²⁹ Thus, as shown in the inset of Fig. S7a,† the HER can be described by a simple equivalent electrical circuit, the solution resistance R_s is approximately 1.1Ω for both electrodes. With respect to R_{ct} , there is a very large difference between the two electrodes. For instance, at $\eta = 100$ mV, R_{ct} is only 2.4Ω for the NFL MoO₂/NF electrode remarkably smaller than that for Ni foam ($\sim 80 \Omega$). The R_{ct} value is strongly related to the kinetics of the HER. The lower the R_{ct} value, the more active the associated electrode for the catalytic reaction.³⁰ Therefore, it is clear that the NFL MoO₂/NF electrode is more active for the catalysis of the HER than the Ni foam electrode. Fig. S8, ESI† shows the polarization curve of NFL MoO₂/NF in 1 M KOH at different temperatures. The HER activation energy of NFL MoO₂/NF is about 20.0 kJ mol^{-1} , according to the Arrhenius equation and Arrhenius plots.³¹ The activation energy of NFL MoO₂/NF is lower than that of other non-precious metal catalysts.^{32–34}

The durability of NFL MoO₂/NF was examined. As shown in Fig. 5a, the NFL MoO₂/NF exhibited a fairly stable performance within the accelerated degradation measurement for 15 000 cyclic voltammetry (CV) cycles between +0.05 and -0.15 V vs. the

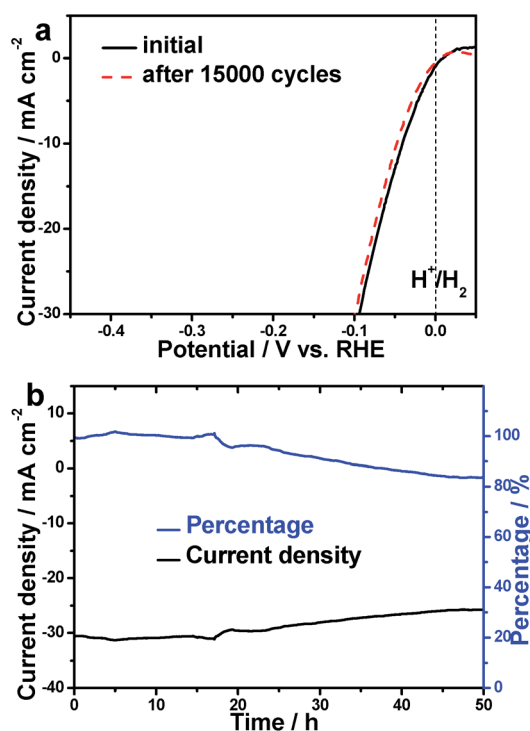


Fig. 5 (a) Polarization curves of the NFL MoO₂/NF in 1 M KOH initially and after 15 000 CV scanning between +0.05 and -0.15 V vs. the RHE. (b) Time-dependent current density curve of NFL MoO₂/NF under a steady-state overpotential of 100 mV for 50 h.

RHE in N₂-saturated 1 M KOH at a scan rate of 50 mV s^{-1} . Fig. 5b shows the time dependent current density and percentage curves for NFL MoO₂/NF under a steady-state overpotential of 100 mV, NFL MoO₂/NF retained 94.3 and 83.6 percent of its initial current density after 25 and 50 hours, respectively. After a long period of time, the current density only slightly degraded, indicating that the NFL MoO₂/NF has superior stability in the long-term electrochemical process.

The superior HER electrocatalytic performance and stability of the NFL MoO₂/NF could be attributed to the following reasons: (1) MoO₂ possesses good electrical conductivity because it has a distorted rutile structure and its bonding involves delocalization of some of the Mo electrons in the conduction band, (2) the nanoflower-like structure of NFL MoO₂/NF could lead to a high surface area, there are correspondingly many active sites exposed for the HER, (3) NFL MoO₂/NF avoids the use of polymer binders which would block active sites, inhibiting diffusion and increasing the time of exposure to air and (4) the porous configuration of Ni foam allows easy diffusion of the electrolyte.

It is important to note that the annealing treatment at 400°C in a H₂ atmosphere is indispensable. With an annealing treatment at 500°C in a N₂ atmosphere, the MoO₂·2H₂O precursor became MoO₂ (Fig. S5†) and the surface of MoO₂ was further oxidized to MoO₃ (Fig. 6b) due to the remains of oxygen in the tube furnace (NFL MoO₂(MoO₃)/NF). A subsequent annealing treatment at 400°C in a H₂ atmosphere was used to reduce the MoO₃ surface of NFL MoO₂(MoO₃)/NF to MoO₂ (NFL MoO₂/NF). Fig. 6a and b show the X-ray photoelectron spectroscopy (XPS) spectra of Mo 3d for NFL MoO₂(MoO₃)/NF and NFL MoO₂/NF, the Mo 3d_{5/2} peak of Mo⁶⁺ was almost coincident with the Mo 3d_{3/2} peak of Mo⁴⁺, thus leading to the characteristic three-peak shape of Mo⁶⁺ and Mo⁴⁺. Treatment at 400°C in a H₂ atmosphere decreased the amount of Mo⁶⁺ at the surface of MoO₂ and the ratio of O/Mo from 2.215 for NFL MoO₂(MoO₃)/NF to 2.077 for NFL MoO₂/NF.

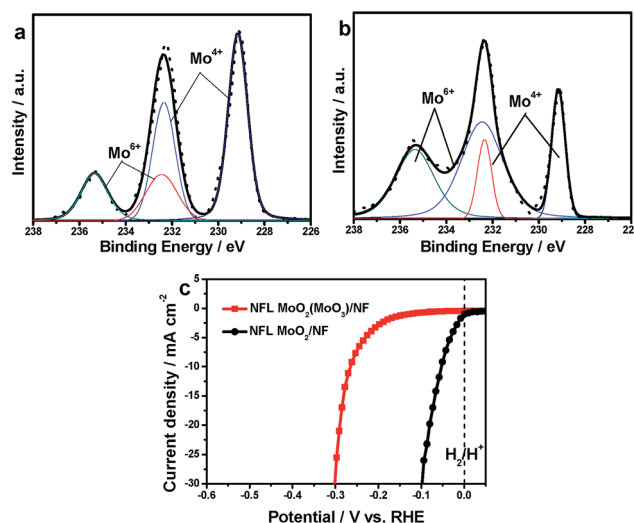


Fig. 6 XPS spectra of Mo 3d for (a) NFL MoO₂/NF and (b) NFL MoO₂(MoO₃)/NF. (c) The polarization curves of NFL MoO₂/NF and NFL MoO₂(MoO₃)/NF in 1 M KOH.

Fig. 6c shows the steady-state polarization curves of NFL MoO₂/NF and NFL MoO₂(MoO₃)/NF in N₂-saturated 1 M KOH solution at 25 °C. In sharp contrast, NFL MoO₂(MoO₃)/NF is less active for the HER with an onset overpotential of about 150 mV. In addition, NFL MoO₂/NF needs an overpotential of only about 55 mV to achieve a current density of 10 mA cm⁻², however, NFL MoO₂(MoO₃)/NF needs an overpotential of about 265 mV to achieve a current density of 10 mA cm⁻². The poor HER performance of NFL MoO₂(MoO₃)/NF could be attributed to the MoO₃ surface, which blocked MoO₂ from coming into contact with the electrolyte. MoO₃ dissolves in alkaline solution and MoO₂ does not dissolve in alkaline solution. Thus, MoO₂ can be stored in alkaline solutions and the MoO₃ surface would dissolve and the MoO₂ would reveal again.

Fig. 6a and Fig. S9, ESI† show the X-ray photoelectron spectroscopy (XPS) data in the Mo 3d and O 1s regions for NFL MoO₂/NF, respectively. It is known that the peaks at ~530 eV are due to oxides and the one at ~532 eV is attributed to adsorbed oxygen. Two peaks at 232.4 and 229.2 eV in the Mo 3d region and peaks at ~530.0 eV in the O 1s region are close to the binding energies of Mo and O in MoO₂. The Mo 3d_{3/2} binding energy of 232.4 eV is positively shifted from that of metallic Mo 3d_{3/2} (231.0 eV) and the Mo 3d_{5/2} binding energy of 229.2 eV is positively shifted from that of metallic Mo 3d_{5/2} (228.0 eV),^{35,36} while the O 1s has a lower binding energy (~530.0 eV) than oxygen (~532 eV). It suggests that the Mo has a partial positive charge (δ^+) but the O has a partial negative charge (δ^-), thus implying the transfer of electrons from Mo to O.^{37–39} A metal complex HER catalyst incorporates proton relays from pendant acid or basic groups, positioned close to the metal center where hydrogen production occurs.^{40,41} Recent work showed that MoP, CoP and FeP as highly active HER catalysts consist of the metal center (δ^+) and the pendant base P (δ^-) close to it.^{37–39} Given that MoO₂ is also rich in metal centers (Mo; δ^+) and pendant bases (O; δ^-) positioned close to it, it is believed that it adopts a catalytic mechanism similar to that of metal complexes, like MoP, CoP and FeP catalysts for the HER. The Mo and basic O act as the hydride-acceptor and proton-acceptor center, respectively, thus facilitating the HER.⁴²

To probe the morphology and composition of the NFL MoO₂/NF after HER electrocatalysis, the SEM, XRD and XPS results of a post-HER NFL MoO₂/NF were collected. As shown in Fig. S10–S11,† the nanoflower-like morphology is preserved and the composition is still MoO₂. Fig. S12† shows the X-ray photoelectron spectroscopy (XPS) spectrum of Mo 3d for NFL MoO₂/NF after HER electrolysis, the amount of Mo⁶⁺ decreased due to the fact that MoO₃ dissolves in alkaline solution.

Conclusions

In conclusion, nanoflower-like MoO₂ has been synthesized successfully for the first time according to our self-developed method. NFL MoO₂/NF showed excellent HER electrocatalytic performance and durability in alkaline electrolytes. The onset potential of NFL MoO₂/NF is almost 0 V *versus* the RHE and bubbles can be seen on the surface under a steady-state overpotential of only 10 mV. NFL MoO₂/NF needs overpotentials of

only about 55 and 80 mV to achieve current densities of 10 and 20 mA cm⁻², respectively.

Acknowledgements

This work was supported by the Major International (Regional) Joint Research Project (51210002), the National Basic Research Program of China (2015CB932304) and the Specialized Research Fund for the Doctoral Program of Higher Education of China (20110171110024). PKS acknowledges the support from the Danish project of Initiative toward Non-precious Metal Polymer Fuel Cells (4106-000012B).

Notes and references

- 1 E. David, *J. Mater. Process. Technol.*, 2005, **162**, 169–177.
- 2 J. D. Holladay, J. Hu, D. L. King and Y. Wang, *Catal. Today*, 2009, **139**, 244–260.
- 3 K. Zeng and D. Zhang, *Fuel*, 2014, **116**, 692–698.
- 4 Y. Sun, M. Delucchi and J. Ogden, *Int. J. Hydrogen Energy*, 2011, **36**, 11116–11127.
- 5 Y. Li, H. Zhang, T. Xu, Z. Lu, X. Wu, P. Wan, X. Sun and L. Jiang, *Adv. Funct. Mater.*, 2015, **25**, 1737–1744.
- 6 Y. Wang, G. Zhang, W. Xu, P. Wan, Z. Lu, Y. Li and X. Sun, *ChemElectroChem*, 2014, **1**, 1138–1144.
- 7 H. Zhang, Y. Li, G. Zhang, T. Xu, P. Wan and X. Sun, *J. Mater. Chem. A*, 2015, **3**, 6306–6310.
- 8 D. Kong, H. Wang, J. J. Cha, M. Pasta, K. J. Koski, J. Yao and Y. Cui, *Nano Lett.*, 2013, **13**, 1341–1347.
- 9 M. A. Lukowski, A. S. Daniel, F. Meng, A. Forticaux, L. Li and S. Jin, *J. Am. Chem. Soc.*, 2013, **135**, 10274–10277.
- 10 Y. Li, H. Wang, L. Xie, Y. Liang, G. Hong and H. Dai, *J. Am. Chem. Soc.*, 2011, **133**, 7296–7299.
- 11 W. Cui, C. Ge, Z. Xing, A. M. Asiri and X. Sun, *Electrochim. Acta*, 2014, **137**, 504–510.
- 12 Z. Pu, Q. Liu, A. M. Asiri, Y. Luo, X. Sun and Y. He, *Electrochim. Acta*, 2015, **168**, 133–138.
- 13 H. Wang, D. Kong, P. Johannes, J. J. Cha, G. Zheng, K. Yan, N. Liu and Y. Cui, *Nano Lett.*, 2013, **13**, 3426–3433.
- 14 H. Vrubel and X. Hu, *Angew. Chem., Int. Ed.*, 2012, **51**, 12703–12706.
- 15 C. Wan, Y. N. Regmi and B. M. Leonard, *Angew. Chem., Int. Ed.*, 2014, **53**, 6407–6410.
- 16 W. F. Chen, C. H. Wang, K. Sasaki, N. Marinkovic, W. Xu, J. T. Muckerman, Y. Zhu and R. R. Adzic, *Energy Environ. Sci.*, 2013, **6**, 943–951.
- 17 W. Cui, N. Cheng, Q. Liu, C. Ge, A. M. Asiri and X. Sun, *ACS Catal.*, 2014, **4**, 2658–2661.
- 18 C. Ge, P. Jiang, W. Cui, Z. Pu, Z. Xing, A. M. Asiri, A. Y. Obaid, X. Sun and J. Tian, *Electrochim. Acta*, 2014, **134**, 182–186.
- 19 J. Kibsgaard and T. F. Jaramillo, *Angew. Chem., Int. Ed.*, 2014, **53**, 14433–14437.
- 20 W. Cui, Q. Liu, Z. Xing, A. M. Asiri, K. A. Alamry and X. Sun, *Appl. Catal., B*, 2015, **164**, 144–150.
- 21 V. Eyert, R. Horny, K. H. Hock and S. Horn, *J. Phys.: Condens. Matter*, 2000, **12**, 4923–4946.

- 22 R. Wu, J. Zhang, Y. Shi, D. Liu and B. Zhang, *J. Am. Chem. Soc.*, 2015, **137**, 6983–6986.
- 23 S. Cheng, H. Liu and B. E. Logan, *Environ. Sci. Technol.*, 2006, **40**, 364–369.
- 24 G. Sasikumar, J. W. Ihm and H. Ryu, *Electrochim. Acta*, 2004, **50**, 601–605.
- 25 J. Tian, Q. Liu, N. Cheng, A. M. Asiri and X. Sun, *Angew. Chem., Int. Ed.*, 2014, **53**, 9577–9581.
- 26 M. Dieterle and G. Mestl, *Phys. Chem. Chem. Phys.*, 2002, **4**, 822–826.
- 27 Y. Liang, Z. Yi, S. Yang, L. Zhou, J. Sun and Y. Zhou, *Solid State Ionics*, 2006, **177**, 501–505.
- 28 S. A. Vilekar, I. Fishtik and R. Datta, *J. Electrochem. Soc.*, 2010, **157**, B1040–B1050.
- 29 D. Merki, H. Vrubel, L. Rovelli, S. Fierro and X. Hu, *Chem. Sci.*, 2012, **3**, 2515–2525.
- 30 N. Krstajić, M. Popović, B. Grgur, M. Vojnović and D. Šepa, *J. Electroanal. Chem.*, 2001, **512**, 16–26.
- 31 K. J. Laidler, *J. Chem. Educ.*, 1984, **61**, 494.
- 32 I. A. Raj and K. Vasu, *J. Appl. Electrochem.*, 1992, **22**, 471–477.
- 33 A. B. Papandrew and T. A. Zawodzinski, *J. Power Sources*, 2014, **245**, 171–174.
- 34 M. De Giz, M. Ferreira, G. Tremiliosi-Filho and E. Gonzalez, *J. Appl. Electrochem.*, 1993, **23**, 641–645.
- 35 E. Minni and F. Werfel, *Surf. Interface Anal.*, 1988, **12**, 385–390.
- 36 B. Brox and I. Olefjord, *Surf. Interface Anal.*, 1988, **13**, 3–6.
- 37 Z. Xing, Q. Liu, A. M. Asiri and X. Sun, *Adv. Mater.*, 2014, **26**, 5702–5707.
- 38 J. Tian, Q. Liu, A. M. Asiri and X. Sun, *J. Am. Chem. Soc.*, 2014, **136**, 7587–7590.
- 39 P. Jiang, Q. Liu, Y. Liang, J. Tian, A. M. Asiri and X. Sun, *Angew. Chem., Int. Ed.*, 2014, **126**, 13069–13073.
- 40 R. H. Newell, D. L. Dubois, A. D. Wilson, M. R. Dubois, M. J. Mcnevin and J. T. Muckerman, *J. Am. Chem. Soc.*, 2006, **128**, 358–366.
- 41 B. E. Barton and T. B. Rauchfuss, *J. Am. Chem. Soc.*, 2010, **132**, 14877–14885.
- 42 J. A. Rodriguez, *J. Am. Chem. Soc.*, 2005, **127**, 14871–14878.